Tribological coatings for complex mechanical elements produced by supersonic cluster beam deposition of metal dichalcogenide nanoparticles

2015 J. Phys. D: Appl. Phys. 48 265302

(http://iopscience.iop.org/0022-3727/48/26/265302)

IOP Publishing

Journal of Physics D: Applied Physics

J. Phys. D: Appl. Phys. **48** (2015) 265302 (13pp)

doi:10.1088/0022-3727/48/26/265302

Tribological coatings for complex mechanical elements produced by supersonic cluster beam deposition of metal dichalcogenide nanoparticles

C Piazzoni[1], M Buttery[2], M R Hampson[2], E W Roberts[2], C Ducati[3], C Lenardi[1], F Cavaliere[1], P Piseri[1] and P Milani[1]

[1] CIMAINA and Dipartimento di Fisica, Università degli Studi di Milano, via Celoria 16, 20133 Milano, Italy
[2] ESTL, ESR Technology Ltd, Whittle House, 410 The Quadrant, Birchwood Park, Warrington, WA3 6FW, UK
[3] Department of Material Science and Metallurgy, University of Cambridge, Cambridge CB3 0FS, UK

E-mail: pmilani@mi.infn.it

Received 11 December 2014, revised 21 April 2015
Accepted for publication 27 April 2015
Published 29 May 2015

Abstract

Fullerene-like MoS_2 and WS_2 nanoparticles can be used as building blocks for the fabrication of fluid and solid lubricants. Metal dichalcogenide films have a very low friction coefficient in vacuum, therefore they have mostly been used as solid lubricants in space and vacuum applications. Unfortunately, their use is significantly hampered by the fact that in the presence of humidity, oxygen and moisture, the low-friction properties of these materials rapidly degrade due to oxidation. The use of closed-cage MoS_2 and WS_2 nanoparticles may eliminate this problem, although the fabrication of lubricant thin films starting from dichalcogenide nanoparticles is, to date, a difficult task. Here we demonstrate the use of supersonic cluster beam deposition for the coating of complex mechanical elements (angular contact ball bearings) with nanostructured MoS_2 and WS_2 thin films. We report structural and tribological characterization of the coatings in view of the optimization of tribological performances for aerospace applications.

Keywords: molybdenum/tungsten disulphide, tribology, nanotechnology, thin films, ball bearings, supersonic cluster beam deposition, 3D coating

(Some figures may appear in colour only in the online journal)

1. Introduction

Molybdenum and tungsten disulfides (MoS_2, WS_2) are compounds belonging to the class of metal dichalcogenides (MX_2 where M = Mo or W and X = S, Te or Se) with a layered structure consisting of stacks of X–M–X sandwiches held together by weak van der Waals interactions [1, 2]. The tendency of weakly bound layers to easily slide one against each other makes MoS_2 and WS_2 materials of great tribological interest [3], in particular for applications in aerospace technology [4] and as additives in fluids for lubrication [5–8].

MS_2 films have a very low friction coefficient in vacuum, therefore they have mostly been used as solid lubricants in space and vacuum applications, mainly in mechanical parts operating in working regimes with either low number of cycles and low speed or low repetition rates [9–11]. Typical examples are the deployment systems for satellites where low friction is required for a low number of cycles, the lubricant must not be a source of vapour phase contamination and it must also withstand high radiation doses, high temperatures and/or large temperature variations [10, 11]. Despite their very attractive structure for solid lubrication, the use of MX_2

films is significantly hampered by the fact that in the presence of humidity, oxygen and moisture, the low-friction properties of these materials rapidly degrade due to oxidation occurring at the boundaries of the X–M–X stacks and lamellas [12, 13].

The laminar structure of MS_2 allows the formation of closed multi-layered structures analogue to carbon fullerenes and nanotubes: these structures are called inorganic fullerenes (IFs) [14] and the resulting solids IF-like materials (IFLMs) [14–16]. Closed-cage structures can limit the oxidation to the outermost layers thus preserving the chemistry and structure of the inner layers, resulting in a reduced overall oxidization of the film [5]. This could favour the in-air lubrication since when entering the contact region these particles break and exfoliate, continuously breeding the interface with un-oxidized sliding layers [17]. IFLM-based coatings are natural candidates for a variety of aerospace applications [18, 19] since good tribological performances in air and in vacuum enable easy and inexpensive in-air pre-test of aerospace mechanisms as well as reduced oxidization can avoid expensive in vacuum pre-launch storage [10, 11].

The synthesis of IF WS_2 and MoS_2 was originally reported by Tenne and co-workers, almost 20 years ago, by heating the corresponding metal films in H_2S gas [14, 15]. In the following years several different physical vapour deposition (PVD) and chemical vapour deposition (CVD) methods have been used to produce IF such as arc discharge under inert atmosphere [20] and water [21], laser ablation [22], sonoelectrochemistry [23], electrochemistry [24], high temperature sulphidation in reducing atmosphere of solid or vapour precursors [16, 25–27], high-irradiance solar furnace [28]. Many of these approaches can produce large quantities of IF nanopowders which can be easily dispersed in liquids. On the other hand the production of thin solid films on surfaces starting from IF nanopowders remains a difficult problem. CVD methods were applied to the production of IF-based coatings, but such coatings suffered, in general, from aggregation/agglomeration of nanoparticles resulting in high friction coefficients. The use of PVD technologies can be beneficial to find a viable solution: on this line we reported the production of nanocomposite thin films consisting of a TiN matrix incorporating IF MoS_2 by coupling reactive arc sputtering for the TiN matrix with supersonic cluster beam deposition (SCBD) of MoS_2 nanoparticles [29].

Here we report the direct and efficient fabrication of pure IF MoS_2 and WS_2 lubricant coatings by SCBD and we demonstrate that this approach can be applied to the production of MX_2 coatings on complex mechanical parts such as angular contact ball bearings commonly employed in a large variety of aerospace applications. The characterization of the structural and morphological properties of nanostructured MX_2 films as a function of the main synthesis and process parameters and their tribological performances is also reported.

2. Experimental

2.1. Nanostructured MS_2 films by cluster-assembling

MoS_2 and WS_2 nanostructured coatings were produced by a SCBD apparatus equipped with two pulsed microplasma cluster sources (PMCSs) [30, 31]. The apparatus consists of three differentially pumped vacuum chambers (figure 1): the first is an expansion chamber (18 dm^3 volume, pumped with a 2000 $l\,s^{-1}$ turbomolecular pump and a 270 $m^3\,h^{-1}$ roots pump) where the supersonic molecular beam is formed. It is connected to a second chamber (11 dm^3 volume, pumped by a 550 $l\,s^{-1}$ turbomolecular pump) by an electroformed skimmer.

The coating deposition takes place in a third deposition chamber (200 dm^3 volume, pumped by a 1000 $l\,s^{-1}$ turbomolecular pump) connected to the rest of the apparatus through a gate valve. A PMCS is mounted outside the expansion chamber on the axis of the apparatus (figure 1); an additional PMCS is mounted off-axis directly on the deposition chamber. A remotely controlled 4-axes manipulator allows for rastering of the sample to guarantee a uniform deposition over a large area. A resistive cartridge heater system can be mounted on the sample holder to heat the substrates in the range RT-300 °C. The deposition chamber also hosts a Kaufman ion gun (Cyberis 40-f) which can be used for either sample cleaning (etching) or co-deposition (sputtering).

The structure of a PMCS is shown in figure 2: it schematically consists of a ceramic body with a channel drilled to perpendicularly intersect a larger cylindrical cavity. The channel hosts a target rod cathode of the material to be vaporized in order to produce the nanoparticles precursors. A solenoid pulsed valve faces one side of the cavity and a removable nozzle closes the other side of it. The valve, backed with a high inert gas pressure (20–50 bars), injects in the source cavity pulses with duration of few hundreds of microseconds at a repetition rate of 3–10 Hz. The nozzle is connected with a series of aerodynamic lenses used to focus neutral nanoparticles on the beam axis [32].

The pulsed injection of the inert carrier gas in the cavity of the PMCS causes the formation of a supersonic jet directed against the target rod. Synchronous with the gas injection a pulsed voltage (50–100 μs of duration, 700–1000 V) is applied to the target cathode and the grounded anode (pulsed valve front) in order to ionize the gas and sputter the target. Due to the plasma confinement obtained by the aerodynamic effects of supersonic expansions, the sputtering process is very efficient and reproducible [31]. The species ablated from the target thermalize with the inert gas and condense to form clusters. The carrier gas-cluster mixture expands out of the nozzle forming a supersonic expansion which impinges on the substrate holder in the deposition chamber [31]. Cluster deposition rate is monitored by a quartz microbalance: rates up to 750 $nm\,h^{-1}$ over a $40 \times 40\,mm^2$ area were obtained depending on the experimental conditions. Coating thickness is characterized after deposition by atomic force microscopy (AFM) and stylus profilometry.

The cathode used to produce MoS_2 (WS_2) nanoparticles consists of a Mo (W) holder rod hosting two MoS_2 (WS_2) drilled cylinders (pellets) and a Mo (W) ring, placed in the centre of the source cavity (figure 2). This setup allowed for overcoming the issues linked to high MS_2 resistivity and mechanical fragility, as either the electrical conductivity or the mechanical stability are supplied by the Mo (W) inserts [29].

Cluster-assembled MoS_2 and WS_2 films were deposited on single crystal 001 silicon slabs, $10 \times 10\,mm^2$, ultrasonically

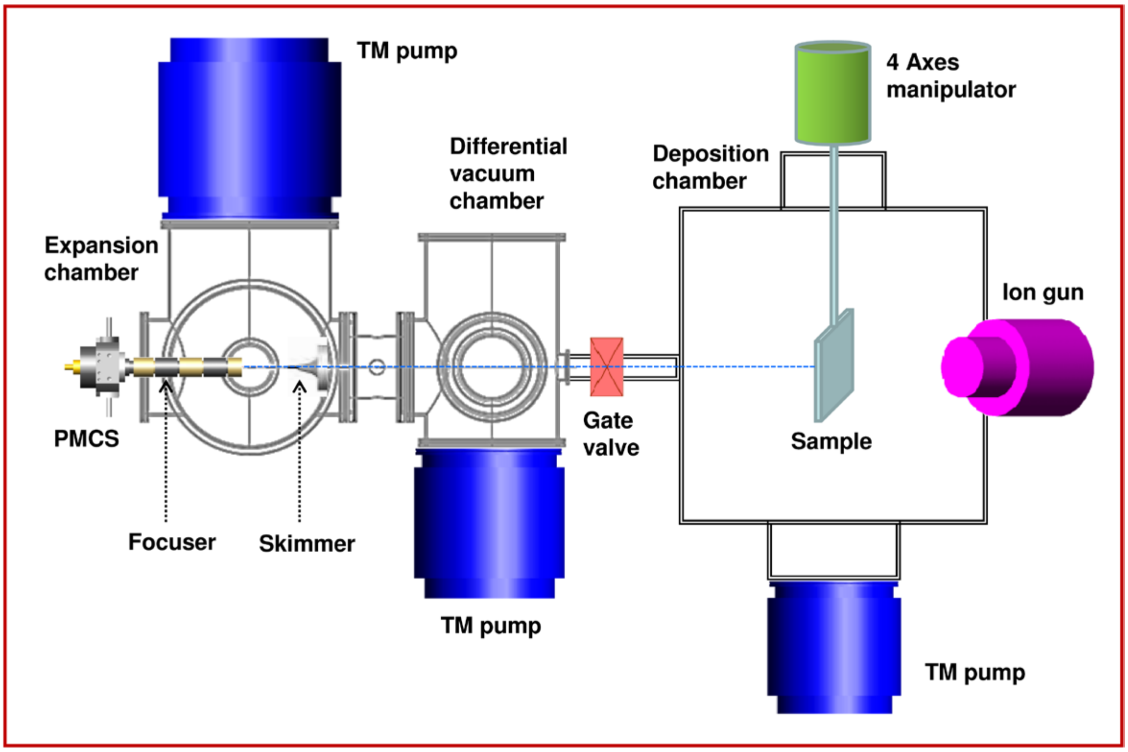

Figure 1. Schematic representation (not to scale) of the SCBD deposition apparatus. Cluster source (PMCS) is mounted on the expansion chamber; a second source (not shown) can be mounted on the deposition chamber.

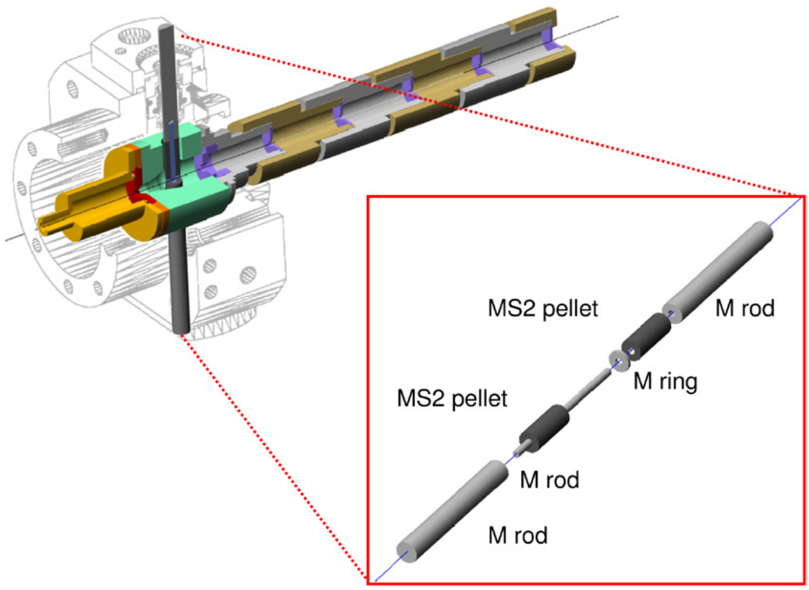

Figure 2. Top-left, PMCS drawing. The target rod ablation takes place in the cavity of the ceramic body (green). The pulsed valve (orange/red) is mounted on the ceramic body; on the opposite side of the cavity the nozzle and the focuser (violet, grey and bronze) are mounted. The number of aerodynamic unit elements (cavity and lens) in the focuser after the first (nozzle) can be varied from 0 to 5. Below-right, composed cathode exploded view.

cleaned in acetone bath for microscopy and spectroscopic characterization.

52100 steel washers, 28/14 mm diameter, polished to a surface roughness of 0.05 μm (Ra) or less were used as substrates for pin on disc (P.o.D.) investigation (figure 3). Washers were ultrasonically cleaned in a mixture of n-propyl bromide and propan-2-ol solvent.

52100 steel angular contact ball bearings (see figure 4) were used as substrates for tribological assessment of coatings deposited on mechanical components. Bearings were ultrasonically cleaned in Lenium ES solvent. Cages were ultrasonically cleaned in isopropyl alcohol (IPA) solvent. Single rings (inner or outer) were coated separately; cages and balls were not coated (see section 2.2).

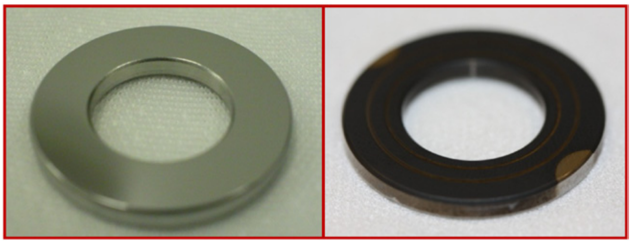

Figure 3. 52100 steel washers used as substrates for pin on disc investigation of coatings. Left, uncoated; right, washer after coating and pin on disc tests (showing uncoated clamper areas and pin scars).

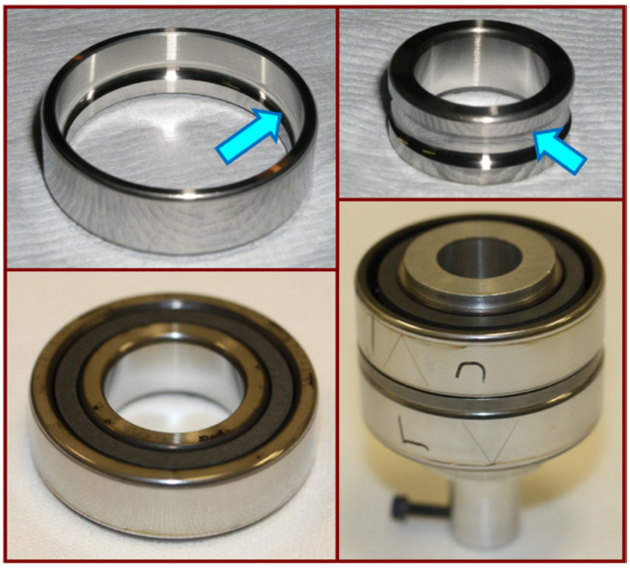

Figure 4. Angular contact bearings (FAG B7004), outer diameter 42 mm, inner diameter 20 mm, 11 balls 6.35 mm diameter, 15° free contact angle; Top-left and top-right, uncoated bearing outer and inner ring: arrows point to the up-to-coat surfaces (races); bottom-left, assembled bearing after races coating (steel spheres are encapsulated in a polymeric brown/grey PGM cage visible between the steel rings); bottom-right, couple of bearings mounted in back to back configuration, set for bearing-rig test.

The main process parameters used to produce different coatings and the corresponding tests performed on them are summarized in table 1.

2.2. Coating of angular contact ball bearings

Ball bearings are commonly used to provide smooth, low friction motion in rotary applications. Ball bearings are composed of four main parts: two rings (inner and outer races) the rolling elements (the balls), and the ball separator (retainer or cage). Due to their spherical shape the balls have minimal contact with the inner and outer races and this allows them to spin smoothly. The outer race mounts into a housing and is stationary. This part also aids in the transfer of the radial load from the bearing to the housing. The inner race mounts onto a rotating shaft and supports and guides the shaft during rotation. The rolling elements carry the load and distribute it throughout the raceways. They rotate around the inner race, but not at the same speed as the rotation of the inner race. The separator acts as a barrier between the balls preventing them from bumping into each other.

In figure 5 we report a schematic representation of the typical ball-bearing assembly to be coated. In the view of cylindrical geometries coating (namely bearing races), a dedicated sample holder/manipulator was developed. As the PMCS is fixed, defining the beam axis, the coating of 3D parts with cylindrical symmetry requires the rotation of the sample in front of the impinging beam (satellite rotation). Furthermore, to reach the internal face of the outer ring, the bearing plane must be tilted while rotating. The tilting also can help to uniformly coat the race of the inner ring.

To perform the satellite movement, a hybrid stepper motor was fixed on a plate hosting the sample shaft on the opposite side and transmitting the rotation through a synchronized belt and pulley system. Rotation of the bearings was remotely controlled via a custom-made Labview interface acting on a unipolar driver board.

2.3. Characterization techniques

Film morphology and elemental composition were characterized by scanning electron microscopy (SEM) and energy dispersive x-ray microanalysis (EDX). AFM (Nanoscope IV operated in Imaging mode) and contact stylus profilometry (Tencor P6) gave additional information on morphology. The AFM was equipped with a standard single crystal silicon tip and the analysis was carried out in air. AFM and profilometer were used to measure the thickness of the deposited films, namely by measurement of steps produced on the samples by masking some sample area. Thickness data were used in connection with quartz microbalance to obtain on line monitoring of the deposition rate.

Transmission electron microscopy (TEM) (FEI Tecnai F20, 200 kV) was used to study the film nanostructure; TEM analysis was performed by removing ns-MS_2 films from Si substrates and dispersing them onto Cu grids for high-resolution TEM. Additional EDX analysis was also performed in TEM mode.

X-ray photoelectron spectroscopy (XPS) was applied to study in detail the chemical composition of films. Photoemission spectra were acquired with ultra-high vacuum (UHV) chamber having a conventional x-ray source (Leybold LHS 10/12 Al Kα = 1486.3 eV). The system is equipped with a hemispherical electron analyser (EA11 MCD). The spectra were acquired in constant pass-energy mode: wide spectra with pass energy E_p = 100 eV, high resolution spectra at the element edges with pass energy E_p = 30 eV. The overall resolution was 0.9 eV. All the spectra are referenced to the Fermi level and the binding energy scale is calibrated via the Au $4f_{7/2}$ core level line (84.0 eV) of a clean polycrystalline Au sample. The line shapes are fitted with mixed singlets obtained by a linear combination of a Gaussian and a Lorentzian profiles sited on a Shirley background.

2.4. Tribological characterization techniques

Tribological tests were performed using a non-vacuum and high-vacuum pin on disc tribometers respectively. The

Table 1. Main process parameters combinations used for coatings production and corresponding test performed (MS = microscopic/spectroscopic, PoD = pin on disc tribology, BB = bearings tribology). IDs M5–9 are grouped here because their relative parameters combinations (concerning etching type and Mo interlayer deposition) proved not significantly different tribological performances.

Material	Coating thickness (nm)	Carrier gas	Temperature (°C)	Cathode central ring thickness (mm)	ID	Test
MoS_2	150	Ar	RT	0.5		MS
			300			
		He	RT			
			300			
	500	Ar	RT		M3	PoD
			100		M4	
		He	RT		M1	
			100		M2	
	1000	He	RT	1	M5–9	PoD, BB (M8 only)
WS_2	150	Ar	RT	0.5		MS
			300			
		He	RT			
			300			
	500	Ar	RT		W2	PoD
			100		W4	
		He	RT		W1	
			100		W3	

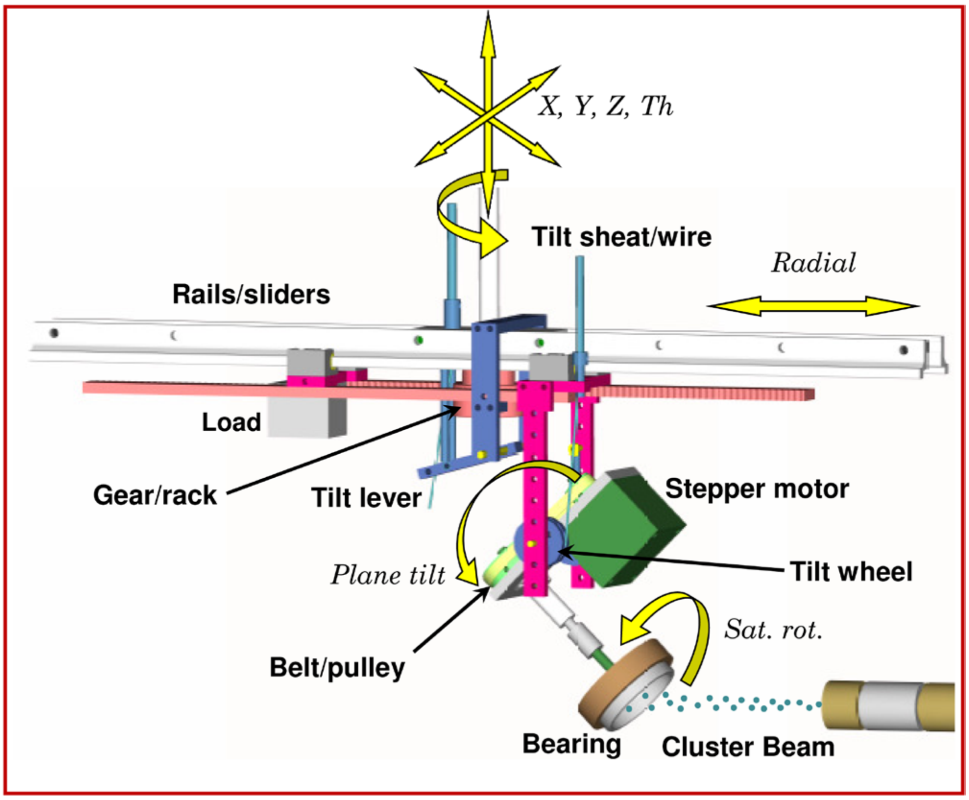

Figure 5. Sample holder for ball bearings coating; yellow arrows show the different degree of freedom of the sample displacement. Outer bearing race coating is presented. The motorized manipulator has the possibility to host two more manual movements. A rotational movement is used to move the sample in the radial direction (centre-periphery of the chamber) on rail sliders through a gear-rack coupling. A twin slider carrying a bare load is moved at the same time in the opposite direction to compensate possible misalignments. A linear movement, acting on a lever, drives a steel wire, sliding through a steel sheath. The wire is fixed onto a wheel bound to the pivoting plate, that holds the motor and the sample. In this way the movement of the lever can be translated into a rotation (tilt) of the sample plane at any radial position. The tilt range is −45° to +90°, fully compliant with races coating needs.

experimental set-ups consisted of a pin mounted on a balanced arm and loaded against the disc by a dead-weight. This set-up is located within an enclosure which can be either purged with nitrogen or evacuated for each tribometer respectively. The disc is rotated by a motor positioned outside the enclosures, and the frictional force is measured by the lateral deflection of the balanced arm. Both tribometers were calibrated by applying known loads to the balanced arm using a pulley system prior to testing.

Pin on disc testing was performed either in laboratory air (class 10 000 environment, RH = 55 ± 10%), or dry nitrogen or high vacuum (<5 × 10^{-6} mbar), at RT using a solvent cleaned, uncoated 7.14 mm diameter 52100 steel ball, loaded to 20 N, providing mean contact stress ~1.00 GPa. The rotation speed was 500 RPM, increased gradually from static. Each test was continued until failure, which was defined as the point at which the coefficient of friction reached a value of 0.3.

Tribological performance of coatings deposited on angular contact bearing races was tested on a dedicated rig under vacuum. Bearings were mounted onto the shaft in a back-to-back configuration (figure 4 bottom-right), and preloaded at 57.5 N via a spring. Motion is controlled via a motor located outside the vacuum chamber. This set-up was calibrated prior to testing by applying known loads to a pivoting arm.

Tests were conducted both in laboratory air (class 10 000 environment, RH = 55 ± 10%) and high vacuum (<5 × 10^{-6} mbar), at RT. The bearings pairs were tested at a speed of 100 RPM until completion of 1 million revolutions (unless premature failure occurred). Assessments of the zero-to-mean and zero-to-peak torque were made through periodic (twice daily) slow speed reversals, consisting of two revolutions cw/ccw/cw at 2RPM.

3. Results and discussion

3.1. Microscopic and spectroscopic investigation of cluster assembled MX_2 coatings

Figure 6(A) shows a SEM micrograph of a standard MoS_2 film deposited by sputtering on silicon substrate: the cross section view evidences a dense columnar structure and a smooth surface, both typical of this kind of coatings.

Figure 6(B) reports SEM micrographs of cluster-assembled WS_2 films of thickness of 150 nm, deposited on silicon substrates. The nanostructured films are characterized by a columnar structure on different length scales typical of ballistic regime deposition. MoS_2 films (not shown) present the same morphology. EDX characterization of MoS_2 and WS_2 films confirmed an average sulphur-to-molybdenum and sulphur-to-tungsten ratio of 1.67 and 1.91 respectively, close to the MS_2 stoichiometry.

Figure 6(B) allows a comparison of WS_2 morphology for films produced with He carrier gas (upper row), Ar carrier gas (central row) both deposited on a substrate kept at room temperature, and Ar carrier gas deposited on a substrate kept art 300 °C (lower row) respectively. A substantial difference between He- and Ar- deposited samples is evident, as the former are composed by small (10–200 nm) and sharp prismatic structures, whereas the latter exhibit a prevalence of larger (up to 800 nm) round-shaped cauliflower structures which, in turn, are composed by smaller (5–10 nm) quasi-spherical particles. These cauliflower structures are preserved in the heated samples, even if their appearance is modified: the overall dimensions are roughly the same, but the roundness of both structures and composing particles is partly lost.

The MoS_2 sputtered film, showed in figure 6(A) as a comparison, has been used (deposited on 52100 steel substrates) as a reference for the tribological characterizations, as reported in sections 3.2 and 3.4.

TEM characterization of WS_2 films deposited at room temperature is showed in figure 7: amorphous and crystalline regions coexist. Straight and curved basal planes series (platelets) and closed nanoparticles are present. Both platelets and particles have the typical WS_2 interplanar spacing of ~0.62 nm [26]. The number of these planes ranges between 5 and 20 in the platelets and 3 and 10 in the particles. Complex nanostructures compatible with double-capped multi-walled nanotube, 120 nm long, 40 nm diam., filled with 10–20 nm nanoparticles (probably metallic W) are observed.

TEM characterization of MoS_2 films deposited at room temperature is showed in figure 8. Images show the same features observed for WS_2 ones, i.e. nanostructures (platelets and particles of 10–150 nm size with interplanar spacing of ~0.63 nm) [33] dispersed in an amorphous matrix. Compared to MoS_2 samples WS_2 films show a wider variety of structures. Furthermore, they can be formed by a larger number of planes which are often rounded and continuously bent whereas MoS_2 platelets and particles have mostly broken corners.

Figure 9 shows a selection of different structures that can be found on WS_2 samples deposited at 300 °C temperature. The substrate heating promotes the appearance of structures such as multi-walled nanotubes, 20–50 nm long, composed by 4–5 0.5 nm-spaced layers and square/rectangular nano-cages, 30–50 nm large, 2–4 layers. In general, in the case of WS_2 films, heating seems to favour the formation of curved platelets and closed structures. The same effect is present but less evident in MoS_2 samples deposited at 300 °C (figure 10). The effect of substrate temperature on the formation of close-caged structures has been reported and discussed in [34].

3.2. Pin on disc characterization

A characterization of the friction coefficient of cluster-assembled MoS_2 films and nano-composites by AFM has been already reported in [29]. AFM is a powerful technique for the assessment of tribological properties at the nanoscale, as discussed in [35]; however in the present case we are interested in the macroscopic performances which are better characterized by pin on disc measurements.

P.o.D. testing of cluster-assembled MoS_2 and WS_2 deposited on 52100 steel washers were conducted in air, nitrogen atmosphere and high vacuum (see section 2.4); results of air and nitrogen tests are reported in figure 11. Data of samples of same material and thickness have been grouped in different graphs [36, 37]. Labels M1–9 and W1–4 refer to different nanostructured MoS_2 and WS_2 coatings produced with the different process parameters combinations listed in table 1. The horizontal dotted lines give a comparison with the performance of reference benchmark coatings, i.e. sputtered MoS_2 and WS_2 of 1 μm thickness [38, 39].

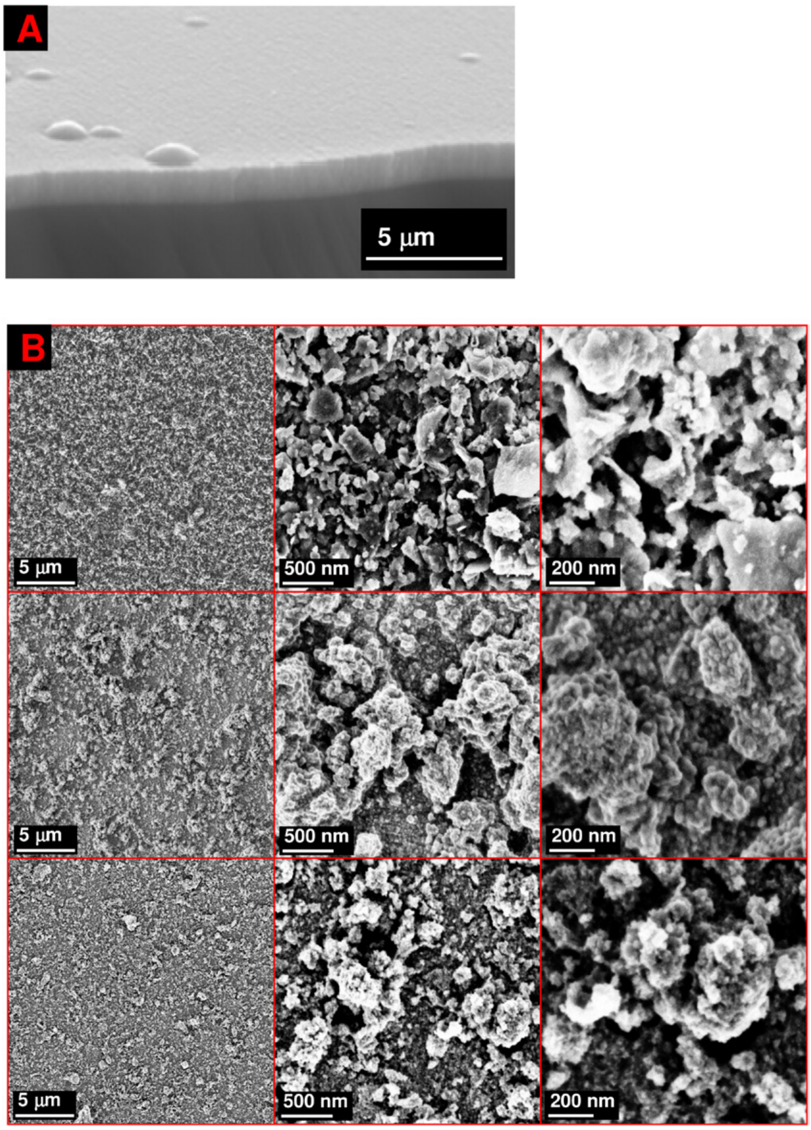

Figure 6. (A) SEM image of RF sputtered MoS_2 sample. (B) SEM images of WS_2 samples. In the first row are reported films deposited with He as carrier gas on a room temperature substrate; centre row reports films deposited with Ar as carrier gas on a room temperature substrate; bottom row reports films as the centre row deposited on a substrate kept at 300 °C.

The cluster-assembled WS_2 coatings (0.5 µm thickness) show considerable variation with different deposition conditions (top-right graph). Whilst the best performing P.o.D. tests can rival standard sputtered WS_2 under nitrogen environment, the lifetime is poor under vacuum. Friction coefficient values are generally comparable to standard WS_2 coatings.

SCDB coatings of 0.5 µm thick MoS_2 also display considerable batch variation (top-left graph). All of them present very low friction coefficients in nitrogen and extremely low friction coefficients in air. Though the best performing coatings did not achieve the sliding lifetimes of the reference sputtered 1 µm MoS_2 coatings, this may be due in part to the reduced coating thickness. Thicker MoS_2 coatings (1 µm) showed significant increases in sliding lifetimes (bottom graph); in particular lifetime in nitrogen was satisfactory for all of the coatings. On the other hand, friction coefficients are good but just slightly better than reference coatings. However the lifetimes are still reduced in comparison with standard MoS_2 in both air and vacuum, with steady-state friction not being achieved for the majority of tests under vacuum. Post-test inspection with an optical microscope revealed failure in all cases to be cause by total removal of the coating.

3.3. XPS analysis of selected coatings

Pin on disc investigation showed that MoS_2 coatings of different thickness had distinctive tribological performance. As evidenced in table 1, coatings of 0.5 µm thickness (M1–M4) are produced using a composite cathode with the central Mo ring of 0.5 mm thickness; on the other side, coatings of 1 µm thickness (M5–M9) are produced using a composite cathode with the central Mo ring of 1 mm thickness. The double thickness of the central Mo ring applied to coatings M5–M9 ensures a better source stability and

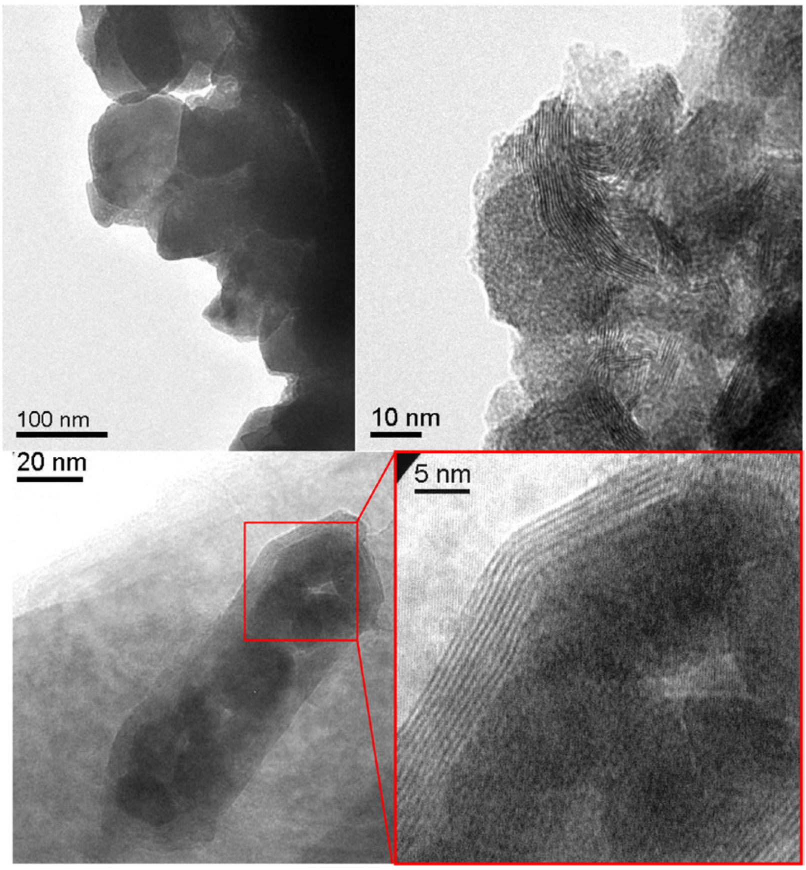

Figure 7. TEM images at different magnifications of WS_2 samples, deposited on room temperature substrates with Ar as carrier gas; down, composite nano-object and detail.

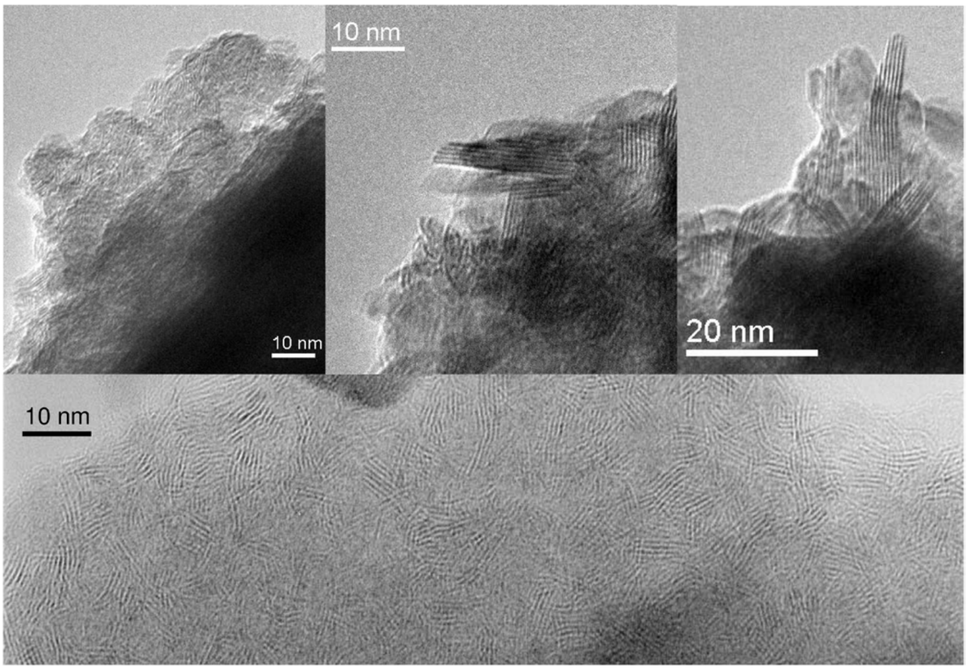

Figure 8. TEM images of MoS_2 samples deposited with He as carrier gas on room temperature substrates.

a higher deposition rate, exploited to easily get a doubled coating thickness.

We selected coatings M2 and M8 as representatives of these categories (table 1 and figure 11) and investigated them by XPS in order to better understand their difference in terms of tribological performances. Samples were analysed as deposited and after *in situ* Ar^+ sputtering (3KV, 1 min) to remove the first coating monolayers, usually suffering from

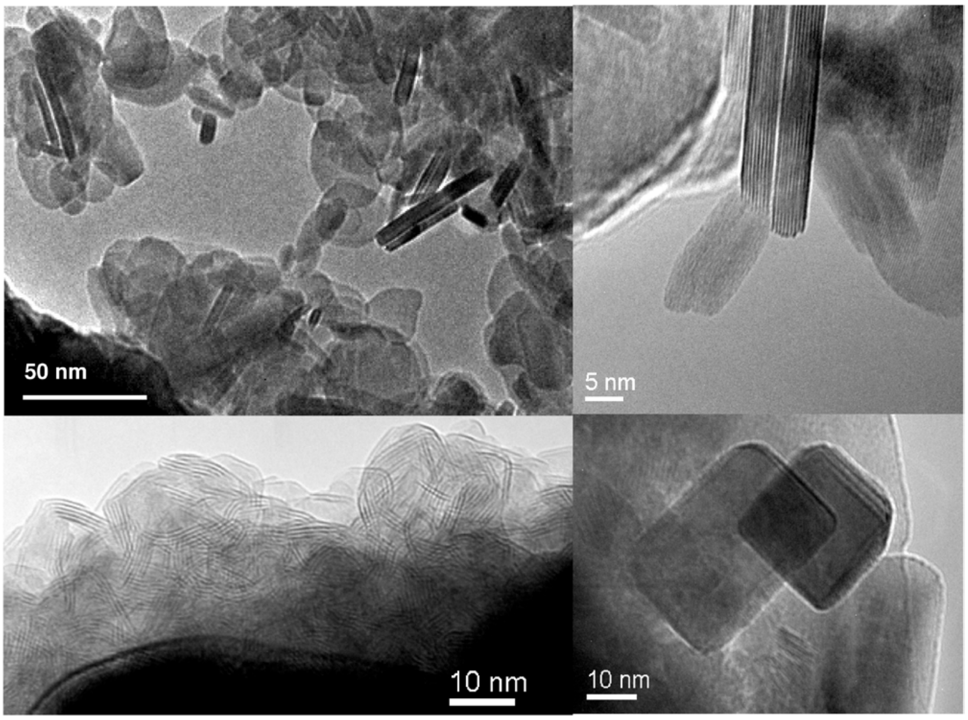

Figure 9. TEM images of WS_2 films deposited with Ar as carrier gas, on substrates heated at 300 °C.

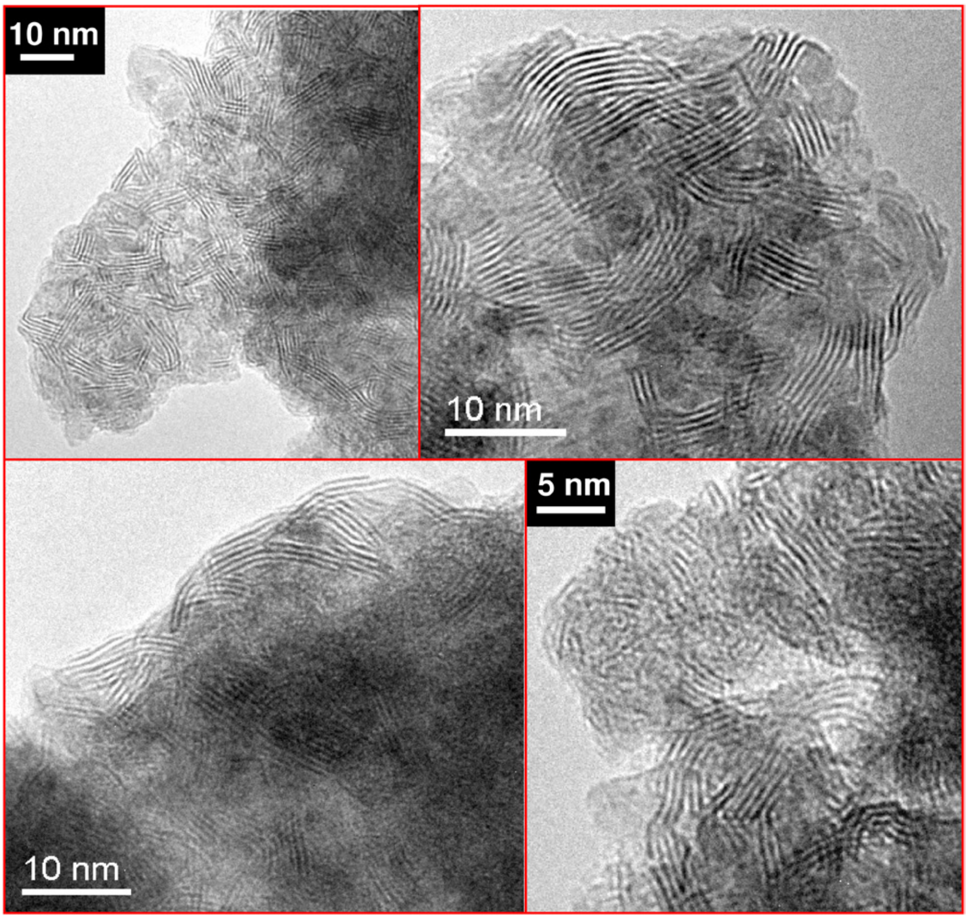

Figure 10. TEM images of MoS_2 samples, deposited with He as carrier gas, on substrates heated at 300 °C.

atmospheric contamination i.e. Mo oxidation and oxygen/water/CO_2 adsorption. The relative abundance of elements and of species bonded to molybdenum is shown in table 2.

XPS analysis evidenced the following aspects: at the surface level the oxygen content is around 50% for both coatings, mainly due to oxygen adsorption after deposition, whereas the

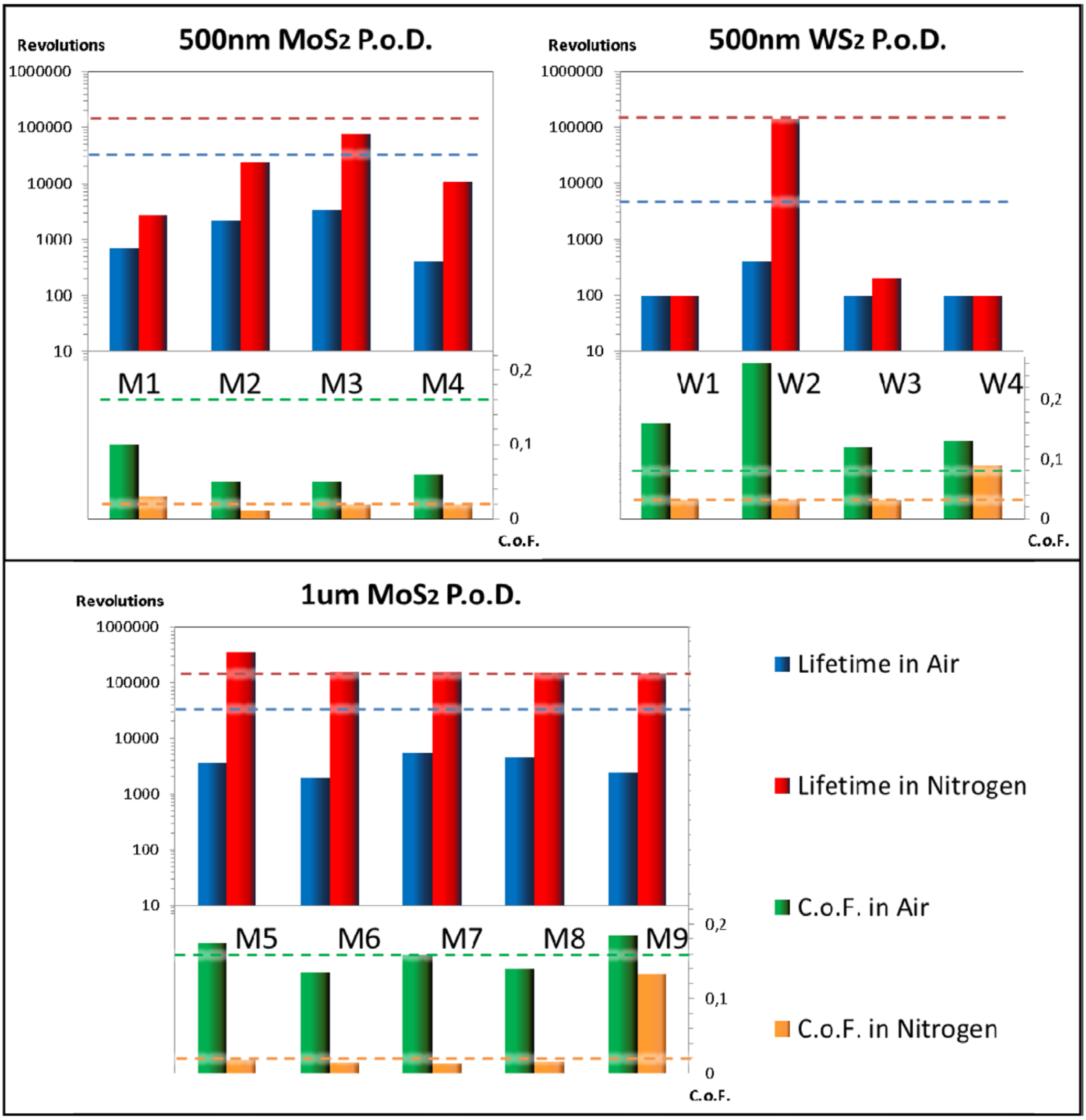

Figure 11. Pin on disc analysis of nanostructured coatings in air and nitrogen atmosphere. Each of the three graphs groups different coatings of same material and thickness and reports lifetimes in the upper part (log scale on left *Y* axis) and coefficients of friction in the lower (linear scale on right *Y* axis). Reference benchmark coatings performances are drawn as dotted horizontal lines; colours of lines and columns correspond to the colours of the parameters listed in the legend.

relative abundance of Mo and S indicates an excess of molybdenum for M8. If we look at the bonded species we can see that in M2 molybdenum is preferentially bonded to sulphur whereas in M8 the molybdenum is evenly bonded to sulphur and to oxygen.

After sputtering, oxygen content is considerably reduced in both of the cases; nevertheless, molybdenum oxides in the M8 case are more than double than in M2 (at around 33%). Other possible contaminations are completely removed. As expected, after the first monolayers removal, the Mo/S ratio is increased in both cases, due to the effect of preferential sputtering of S with respect to Mo [40]. Nevertheless we can see that in depth (i.e. without contaminations contributions) the differences in the elemental composition of the two samples are more evident than at the surface: coating M2 shows a reduced oxygen content and an almost correct proportion of Mo and S; whilst in coating M8 the molybdenum is dominant, the oxygen content is still relevant and the sulphur content is largely under-stoichiometric.

Either the increase of the MoO_x phase or the presence of not-stoichiometric MoS_x are possible causes of the rise of coefficient of friction observed in the M8 case.

The XPS analysis combined to pin on disc results suggest that the use of 1 mm thick Mo ring in the composite cathode

Table 2. XPS quantitative analysis evaluated by acquiring the Mo3d, O1s and S2p edges. Upper rows: relative abundance of elements before and after sputtering. Lower rows: relative abundance of molybdenum-sulphur and molybdenum-oxygen species before and after sputtering.

	Relative abundance (at.%)			
	Coating M2		Coating M8	
Elements	Surface	After sputtering	Surface	After sputtering
Mo	14.78	33.57	26.42	54.32
O	50.56	10.15	52.70	27.98
S	34.66	56.28	20.87	17.71
Bonded species				
MoS_x	45.67	81.60	37.83	58.67
MoO_x	28.36	14.27	39	32.82

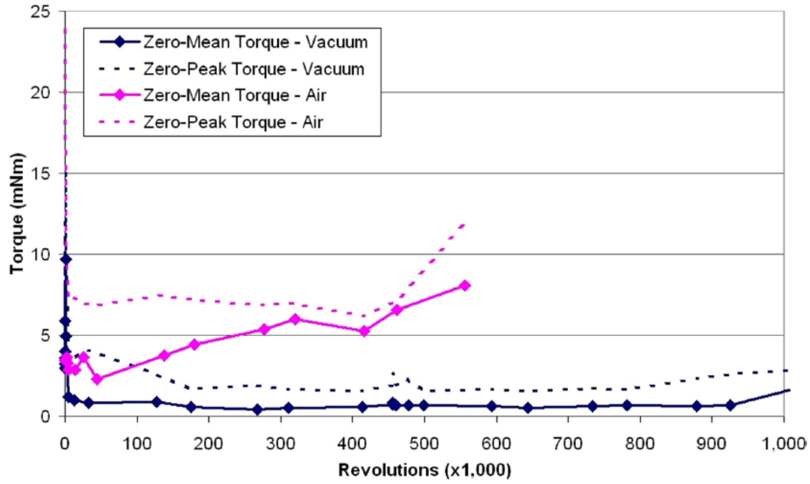

Figure 12. Torque behaviour of bearings with SCBD MoS_2 on raceways, fitted with PGM cages, running under vacuum and in air.

(applied to M5-M9 coatings) is beneficial to easily increase the final coating thickness, thus determining an increased lifetime; on the other side, it results in a different chemical composition of the coating that reduces the excellent coefficient of friction performances reached by coatings produced with 0.5 mm ring (M1–M4).

3.4. Angular contact bearing testing

Due to the better lifetime and repeatability of results in terms of coating thickness and tribological performance, M8 coating was selected for deposition on angular contact bearings (see section 2.2). Pre-test inspection revealed that the cluster-assembled MoS_2 coating was well adherent and uniform on the inner and outer bearing raceways. Bearings were preloaded to 57.5 N in a back-to-back arrangement, with one pair being operated under vacuum, and a second pair being run in-air. Cage retainers were procured of PGM, a self-lubricating composite of polytetrafluoroethylene (teflon) (PTFE), glass fibres and MoS_2 commonly used in conjunction with sputtered MoS_2. Bearings tests results are presented in figure 12.

The results of the in-vacuum bearing test demonstrated that cluster-assembled MoS_2 is capable of lubricating under such conditions for a duration of 1 million revolutions. Mean and peak torque values were generally steady throughout the test and within the range expected for sputtered MoS_2 (~1 mNm zero-mean torque). Occasional high torque excursions were observed, but these increases are believed to be a result of the PGM-material transfer to the balls. In all such cases low torque was re-achieved after a period of a few thousand bearing revolutions. Torque values and noise did show systematic increase in the final stages of the test, from 900 000 revolutions onwards.

Post-inspection of the bearings showed the upper bearing to be in good condition, with MoS_2 still present on the bearing rings. However a small amount of steel wear was observed within the lower bearing, with no MoS_2 remaining in the ball tracks. This observation was verified by SEM/EDAX analysis of the raceways, suggesting that the increase in torque seen around 950 000 revolutions was due to the removal of MoS_2 coating from the lower bearing. Given the small volume of wear debris, and the low torque during the majority of the bearing test, we conclude that this coating removal occurred very shortly before the test was stopped, and that prolonged steel-steel running had not occurred.

The bearing test in air showed mean torque levels being several times higher than those running under vacuum, and low (<4 mNm) torque only being measured for the first ~150 000 revolutions. Bearings also displayed high torque noise throughout the test. The test was stopped after 550 000 revolutions. Post-test inspection revealed removal of the MoS_2 from the ball tracks, and clear evidence of running without lubrication.

5. Conclusions

Nanostructured MoS_2 and WS_2 coatings for tribological applications have been produced by SCBD: the structure and morphology of the films was investigated as a function of different production parameters. SCBD technique was successfully applied to the coating of mechanical components of complex geometry (angular contact bearings) by means of a multi-axis sample holder manipulator.

Pin on disc investigation was used to characterize the coating performances as lubricant of the bearing races. Cluster-assembled MoS_2 showed very good performances in terms of friction coefficient compared to standard films both in nitrogen and in air; however this was at the expenses of lifetime: in fact when the nanostructured coating thickness is increased in order to increase the lifetime, also the friction coefficient increases. This can be motivated by considering that XPS analysis showed a clear correlation between the chemical composition and the lubrication activity of the coatings: thicker nanostructured films contain a larger amount of unreacted molybdenum and its oxides which lower the quality of the tribological performances. In order to reach performances beyond the classical coatings, an optimization of the deposition parameters is necessary to prevent the presence of metal oxides while having a large thickness. This will allow to deposit nanostructured films with improved lifetime while keeping low friction coefficient.

The bearing test results showed good performance in vacuum and poor performance in air, at odd with the trend of the pin on disc tests. This difference may be due to the different lubricating regimes; sliding for the P.o.D., predominantly rolling in the bearings. Alternatively this could be a stress factor; the mean contact stress in the P.o.D. tests was approximately twice that of the bearing tests, and may represent some upper stress limit in the lubricating properties of such nano-fullerene structured lubricants.

Our results represent the proof of principle that SCBD can be used for the production of nanostructured coatings obtained from metal dichalcogenide nanoparticles on complex 3D components in view of tribological applications.

Acknowledgments

We thank G. Lo Sacco for assistance in the XPS characterizations. This work has been financially supported by the EC under the project ‘FOREMOST—Fullerene-based Opportunities for Robust Engineering: Making Optimised Surfaces for Tribology’ (Contract no.: FP6-515840) and by ESA under the ITI projects ‘Tribological Study of Cluster Beam Deposited Inorganic Nano-Fullerene Materials’ (ESA ESTEC/Contract No. 20816/07/NL/CB) and ‘Nano-Structured Lubricants for Bearing Applications in Space’ (ESA ESTEC/Contract No. 22287/09/NL/CBI). The research leading to these results has received funding from the European Union Seventh Framework Programme under Grant Agreement 312483—ESTEEM2 (Integrated Infrastructure Initiative–I3), CD authors acknowledges funding from the ERC under grant number 259619 PHOTO EM.

References

[1] Shriver D F and Atkins P W 1999 *Inorganic Chemistry* 3rd edn (Oxford: Oxford University Press) pp 638–9
[2] Wilson J A and Yoffe A D 1969 The transition metal dichalcogenides discussion and interpretation of the observed optical, electrical and structural properties *Adv. Phys.* **18** 193–335
[3] Cizaire L, Vacher B, Le Mognea T, Martina J M, Rapoport L, Margolinc A and Tenne R 2002 Mechanisms of ultra-low friction by hollow inorganic fullerene-like MoS_2 nanoparticles *Surf. Coat. Technol.* **160** 282
[4] Roberts E W 1990 Thin solid lubricant films in space *Tribol. Int.* **23** 95
[5] Rapoport L, Feldman Y, Homyonfer M, Cohen H, Sloan J, Hutchison J L and Tenne R 1999 Inorganic fullerene-like material as additives to lubricants: structure-function relationship *Wear* **225–229** 975–82
[6] Arbabi H and Eyre T S 1986 Investigation into the lubricating effectiveness of molybdenum-disulfide dispersion in a fully formulated oil *Tribol. Int.* **19** 87–91
[7] Demas N G *et al* 2012 Tribological effects of BN and MoS_2 nanoparticles added to polyalphaolefin oil in piston skirt/cylinder liner tests *Tribol. Lett.* **47** 91–102
[8] Risdon T J, Sinsheimer J D and Landry D K 1991 Effect of MoS_2 on corrosion inhibition of NLGI reference grease *Tappi J.* **74** 220–4
[9] Spalvins T 1987 A review of recent advances in solid film lubrication *J. Vac. Sci. Technol.* A **5** 212
[10] Hilton M R and Fleischauer P D 1992 Applications of solid lubricant films in spacecraft *Surf. Coat. Technol.* **54/544** 435
[11] Voevodin A A and Zabinski J S 2005 Nanocomposite and nanostructured tribological materials for space applications *Compos. Sci. Technol.* **65** 741–8
[12] Singer I L, Fayeulle S and Ehni P D 1996 Wear behavior of triode-sputtered MoS_2 coatings in dry sliding contact with steel and ceramics *Wear* **195** 7
[13] Wahl K J, Belin M and Singer I L 1998 A Triboscopic investigation of the wear and friction of MoS_2 in a reciprocating sliding contact *Wear* **214** 212
[14] Tenne R, Margulis L, Genut M and Hodes G 1992 Polyhedral and cylindrical structures of tungsten disuphide *Nature* **360** 444
[15] Margulis L, Salitra G, Tenne R and Talianker M 1993 Nested fullerene-like structures *Nature* **365** 113
[16] Feldman Y, Wasserman E, Srolovitz D J and Tenne R 1995 High-rate, gas-phase growth of MoS_2 nested inorganic fullerenes and nanotubes *Science* **267** 222
[17] Alberdi A, Hatto P, Diaz B and Csillag S 2011 Tribological behavior of nanocomposite coatings based on fullerene-like structures *Vacuum* **85** 1087–92
[18] Miyoshi K 2001 Durability evaluation of selected solid lubricating films *Wear* **251** 1061–7
[19] Ye Y, Chen J and Zhou H 2009 An investigation of friction and wear performances of bonded molybdenum disulfide solid film lubricants in fretting conditions *Wear* **266** 859–64
[20] Chhowalla M and Amaratunga G A J Thin films of fullerene-like MoS_2 nanoparticles with ultra-low friction and wear 2000 *Nature* **407** 164
[21] Sano N, Wang H, Chhowalla M, Alexandrou I, Amaratunga G A J, Naito M and Kanki T 2003 Fabrication of inorganic molybdenum disulfide fullerenes by arc in water *Chem. Phys. Lett.* **368** 331
[22] Parilla P A, Dillon A C, Jones K M, Riker G, Schulz D L, Ginley D S and Heben M J 1999 The first true inorganic fullerenes? *Nature* **397** 114

[23] Mastai Y, Homyonfer M, Gedanken A and Hodes G 1999 Room temperature sonoelectrochemical synthesis of molybdenum sulfide fullerene-like nanoparticles *Adv. Mater.* **11** 1010
[24] Ponomarev E A, Albu-Yaron A, Tenne R and Levy-Clement C 1997 Electrochemical deposition of quantized particle MoS_2 thin films *J. Electrochem. Soc.* **144** L277
[25] Feldman Y, Frey G L, Homyonfer M, Lyakhovitskaya V, Margulis L, Cohen H, Hodes G, Hutchison J L and Tenne R 1996 Bulk synthesis of inorganic fullerene-like MS_2 (M) Mo, W) from the respective trioxides and the reaction mechanism *J. Am. Chem. Soc.* **118** 5362
[26] Yang H *et al* 2006 Synthesis of inorganic fullerene-likeWS_2 nanoparticles and their lubricating performance *Nanotechnology* **17** 1512
[27] Sadale S B *et al* 2006 Synthesis of type-I textured tungsten disulfide thin films on quartz substrate *J. Cryst. Growth* **286** 481
[28] Gordon J M, Katz E A, Feuermann D, Albu-Yaron A, Levy M and Tenne R 2008 Singular MoS_2, SiO_2 and Si nanostructures—synthesis by solar ablation *J. Mater. Chem.* **18** 458–62
[29] Piazzoni C *et al* 2008 Nanocomposite TiN films with embedded MoS_2 inorganic fullerenes produced by combining supersonic cluster beam deposition with cathodic arc reactive evaporation *Appl. Phys.* A **90** 101–4
[30] Milani P and Iannotta S 1999 *Synthesis of Nanophase Materials by Cluster Beam Deposition* (Berlin: Springer)
[31] Barborini E, Piseri P and Milani P 1999 A pulsed microplasma source of high intensity supersonic carbon cluster beams *J. Phys. D: Appl. Phys.* **32** L105
[32] Piseri P, Vahedi-Tafreshi H and Milani P 2004 Manipulation of nanoparticles in supersonic beams for the production of nanostructured materials *Curr. Opin. Solid State Mater. Sci.* **8** 195–202
[33] Dunn D N, Seitzman L E and Singer I L 1998 MoS_2 deposited by ion beam assisted deposition: 2H or random layer structure? *J. Mater. Res.* **13** 3001
[34] Chang L *et al* 2006 Simple synthesis and characteristics of Mo/MoS_2 inorganic fullerene-like and actinomorphic nanospheres with core-shell structure *Nanotechnology* **17** 3827–31
[35] Buzio R, Gnecco E, Boragno C and Valbusa U 2002 Friction force microscopy investigation of nanostructured carbon films *Carbon* **40** 883
[36] Piazzoni C and Hampson M 2008 Tribological study of cluster beam deposited inorganic nano-fullerene materials ITI-ESTL-0178-08
[37] Piazzoni C and Buttery M 2010 Nano-structured lubricants for ball bearing applications in space ITI-ESTL-TM-0076
[38] Friction and wear properties of newly developed solid lubricant coatings ESA-ESTL-TM-0048 01
[39] Roberts E W Optimisation of WS_2 deposition for thin film solid lubrication ESA-ESTL-TM-0067 01
[40] Baker M A, Gilmore R, Lenardi C and Gissler W 1999 XPS investigation of preferential sputtering of S from MoS_2 and determination of MoS_x stoichiometry from Mo and S peak positions *Appl. Sur. Sci*. **150** 255–62